(Received 1 September 2025, Accepted 15 October 2025, Scheduled 29 October 2025)

Long-Medium Range Millimeter-Wave Microstrip Array based on SIW Feeding Network for Automotive Radar Applications

Yan Sun, Dan Zhang*, Jiazi Liu, and Zhiqi Li

College of Information Science and Technology, Nanjing Forestry University, Nanjing 210037, China

ABSTRACT: This paper introduces a substrate-integrated waveguide (SIW)-fed broadband antenna array employing proximity-coupled radiating elements for automotive radar applications. The design integrates three key innovations: (1) a periodic staggered arrangement of hybrid rectangular-polygonal patches, (2) combined proximity coupling with reflective slot structures enabling simultaneous broadband impedance matching and sidelobe suppression, and (3) an optimized 8×28 planar configuration operating at 77–81 GHz. Measurements of the fabricated prototype demonstrate an 8.86% impedance bandwidth (75.2–82.2 GHz) with dual-beam radiation characteristics — achieving a narrow beam ($\pm 5.5^\circ$) for long-range detection and a wide beam ($\pm 30.4^\circ$) for medium-range scenarios. The antenna maintains sidelobe levels below -20 dB, peak gain exceeding 19.8 dBi, and gain fluctuation within 1 dB across the operational band. Notably, the hybrid patch geometry and slot-loading technique yield a flattened radiation pattern with suppressed sidelobes, outperforming conventional mmWave arrays in radiation stability. The compact architecture demonstrates strong potential for next-generation automotive radars requiring high-resolution target discrimination.

1. INTRODUCTION

Millimeter-wave (mmWave) radar has been widely adopted in automotive applications with the rapid development of autonomous driving and intelligent transportation systems [1, 2]. Compared with LiDAR and vision-based sensors, mmWave radar offers stronger resistance to environmental interference, accurate velocity and distance measurements, and reliable all-weather operation [3], making it a critical component of modern vehicular perception systems.

Automotive radars are generally classified by detection range into short-range radar (SRR), medium-range radar (MRR), and long-range radar (LRR) [4–6]. SRR is typically employed for blind spot detection and parking assistance, while MRR and LRR support advanced driver-assistance systems (ADASs), including adaptive cruise control (ACC), lane change assistance, and collision avoidance. Among available spectrum allocations, the 77–81 GHz band has become the dominant choice for MRR and LRR due to favorable propagation characteristics and international regulatory acceptance [4, 7].

Within this band, MRR and LRR antenna requirements differ significantly in azimuthal field of view (FoV) and detection range, and no unified industry standard exists [8]. Reported designs indicate typical -3 dB beamwidths of $\pm 15^\circ$ for LRR and $\pm 40^\circ$ for MRR in the azimuth plane, with both maintaining $\pm 5^\circ$ in elevation. LRR systems generally adopt narrow-beam, high-gain antennas for long-range precision, whereas MRR systems utilize wide-beam arrays for broader coverage [9–11].

As shown in Fig. 1, conventional approaches employ separate MRR and LRR modules, each optimized for distinct beam patterns [12–14]. For continuous FoV coverage, such systems require rapid mode switching, with maximum detection ranges denoted as R_{MRR} and R_{LRR} [15]. However, frequent switching may introduce latency in safety-critical environments, where radar signal processing must operate in real time. An integrated medium- and long-range radar (LMRR) antenna is therefore desirable, providing simultaneous narrow beams for long-range detection and wide beams for medium-range coverage, along with wide bandwidth, high gain, low sidelobe levels, and stable performance across the 77–81 GHz band.

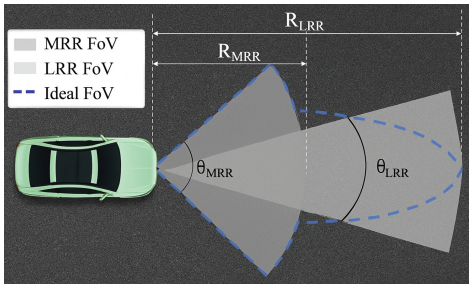

FIGURE 1. Ideal FoV for medium- and long-range automotive radar.

This work proposes a substrate-integrated waveguide (SIW)-based antenna array architecture for integrated mid- and long-range automotive radar. The design combines a proximity-coupled radiating structure with a custom SIW 1-to-8 unequal power divider, extended into an 8×28 planar array to support simultaneous MRR and LRR operation. The array employs staggered hybrid patch elements, standing-wave excitation, and reflective slots to achieve broadband impedance matching and effective beam shaping. A prototype was fabricated and experimentally characterized, with results discussed in subsequent sections to demonstrate the feasibility of the proposed approach.

* Corresponding author: Dan Zhang (zhangdan@njfu.edu.cn).

2. ANTENNA DESIGN AND ANALYSIS

2.1. 28-Element Parasitic Radiation Structure Design

The proposed radiator structure is fabricated on a Rogers RO3003 substrate with a thickness of 0.127 mm, a relative dielectric constant $\varepsilon_r = 3.0$, and a loss tangent $\tan\delta = 0.0013$ [16].

Figure 2 illustrates the configuration of the proposed microstrip radiator with 28 parasitic elements. The structure is patterned on the top layer of the printed circuit board (PCB), with a solid ground plane on the backside, and contains no vias. The radiator consists of a central microstrip feed line with width w_f, multiple rectangular radiating elements sharing the same bottom width but with different heights (Q_1, Q_2, Q_3), and polygonal patches characterized by bottom width a, top width b, side length t, and height h. Two adjacent rectangular patches of identical shape and size form a "radiating element group," while each polygonal patch independently constitutes a separate "radiating element group." These groups are arranged periodically and in a staggered manner on both sides of the microstrip line, maintaining a fixed lateral spacing L_n from the feed line.

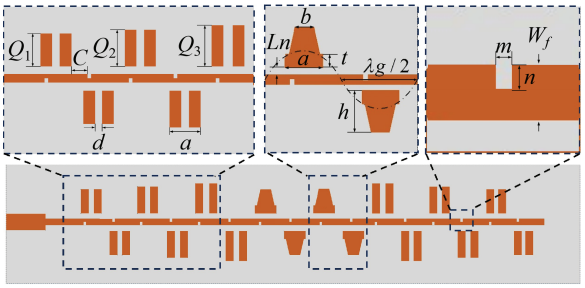

FIGURE 2. Radiating structure with 28 elements. The dimensions are: $a = 1.15$, $b = 0.2$, $h = 1$, $d = 0.16$, $m = 0.078$, $n = 0.121$, $L = 20.5$, $W_f = 0.28$, $C = 0.1$, $Q_1 = 1$, $Q_2 = 1.12$, $Q_3 = 1.6$, $r = 0.64$ (unit: mm).

When the end of the microstrip line is open-circuited, the radiator operates in a standing-wave mode, wherein the radiating elements are effectively excited via proximity electromagnetic coupling from the feed line [17, 18]. To ensure in-phase excitation across the radiator, the spacing between adjacent radiating element groups is precisely set to half of the guided wavelength, i.e., $\lambda_g/2$. Additionally, $m \times n$ reflective slots are introduced along the microstrip feed line to suppress undesired wave refraction and enhance beam-shaping performance.

The 28-element radiator can be modeled as a parallel RLC circuit to explain its impedance matching and band-pass characteristics. The distance between the radiating element and feed line (L_n) is a key parameter; increasing L_n reduces the coupling strength, which shifts the resonance frequency upward and broadens the impedance bandwidth. This behavior is confirmed by the simulated S_{11} results shown in Fig. 3.

By utilizing a two-port network analysis approach with S-parameters, the influence of the feed line can be effectively eliminated. The normalized impedance R_n at the center of the patch can be represented by $|S_{11}|$ as follows:

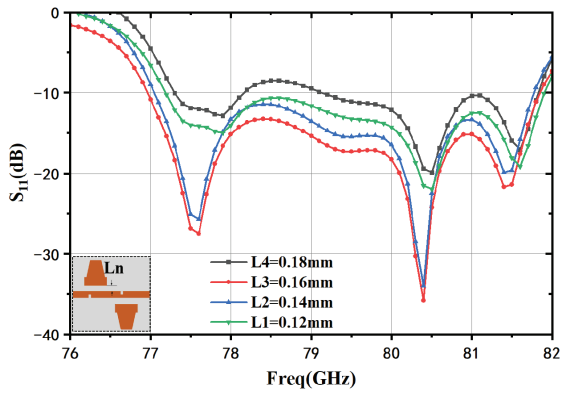

FIGURE 3. Simulated S_{11} under different values of L_n.

$$R_n = \frac{Z_n}{Z_0} = \frac{2S_{11}}{1 - S_{11}} \tag{1}$$

As the distance L_n between the radiating element and feed line increases, the coupling energy decreases, leading to a reduction in the normalized impedance R_n.

As shown in Fig. 4, With rectangular reflector slots introduced near the coupling ports, the radiator achieves sidelobe flattening through destructive interference while simultaneously enhancing impedance matching and broadening the S_{11} bandwidth.

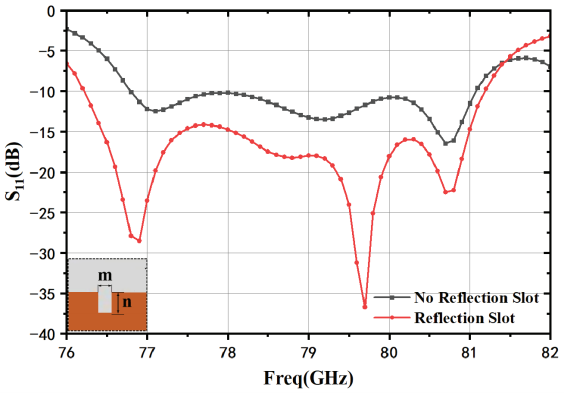

FIGURE 4. S_{11} simulation with and without reflective grooves.

2.2. 8×28 Medium-and-Long-Range Planar Array

An 8×28 planar array with a substrate integrated waveguide (SIW)-based feeding network was designed for the 77–81 GHz band. The feeding network employs an unequal power divider and phase shifters to regulate power distribution and beamforming. Port 1 serves as the feeding input, while Ports 2–9 are the output ports. Symmetrical via-loaded branches and optimized channel widths are implemented to enhance bandwidth and ensure uniform excitation, and the SIW feeding network is integrated with the backside ground plane through metallic vias. By optimizing the spatial distribution and geometric parameters of the vias, precise control of the excitation current distribution can be achieved, and the detailed structure is shown in Fig. 5.

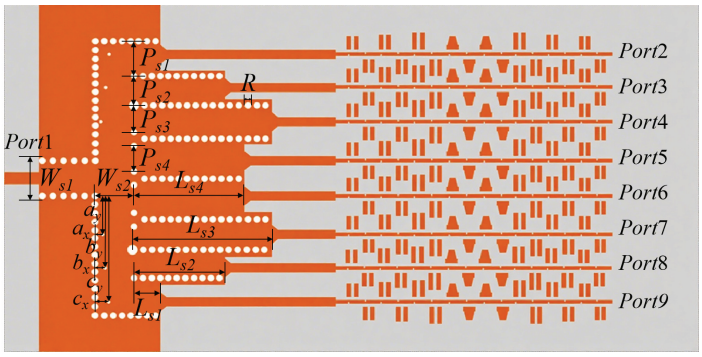

FIGURE 5. Structure of 8×28 Broadband LMRR Planar Array Antenna. Dimensions of the SIW feed network are: $W_{s1} = 2.3$, $W_{s2} = 2.2$, $L_{s1} = 2.0$, $L_{s2} = 6.6$, $L_{s3} = 9.1$, $L_{s4} = 7.2$, $P_{s1} = 2.2$, $P_{s2} = 2.2$, $P_{s3} = 1.72$, $P_{s4} = 1.47$, $a_x = 0.45$, $a_y = 2.47$, $b_x = 0.55$, $b_y = 4.67$, $c_x = 0.83$, $c_y = 6.87$, $R = 0.4$ (unit: mm).

The SIW exhibits similar electromagnetic wave propagation characteristics to conventional rectangular waveguides, and its cutoff frequency can be determined from the waveguide width W [19–22].

$$\bar{\alpha} = \varepsilon_1 + \frac{\varepsilon_2}{\frac{s}{2r} + \frac{\varepsilon_1 + \varepsilon_2 - \varepsilon_3}{\varepsilon_3 - \varepsilon_1}} = \frac{W_{eff}}{W} \tag{2}$$

$\bar{\alpha}$ denotes the normalized width of the equivalent rectangular metallic waveguide, s the spacing between adjacent vias, and r the via radius. Parameters ε_1, ε_2, and ε_3 correspond to the relative permittivity of the substrate, the effective permittivity of the microstrip line, and the effective permittivity of the SIW structure, respectively. Additionally, W_{eff} refers to the equivalent waveguide width of the SIW, and λ_g denotes the guided wavelength within the SIW.

$$\lambda_g = \frac{\lambda}{\sqrt{1 - \left(\frac{\lambda}{2W_{eff}}\right)^2}} \tag{3}$$

$$\beta_m(f) = \frac{2\pi\sqrt{\epsilon_e} f}{300} \tag{4}$$

$$\beta_{siw}(f) = \sqrt{\left(\frac{2\pi\sqrt{\epsilon_r} f}{300}\right)^2 - \left(\frac{\pi}{W_{eff}}\right)^2} \tag{5}$$

ε_e denotes the effective dielectric constant of the microstrip line, f the operating frequency, and W_{eff} the equivalent waveguide width. Let L_{siw} and L_m be the lengths of the SIW section and microstrip section, respectively. The total phase variation of the composite structure is then expressed as:

$$\varphi(f) = \beta_{\text{siw}} L_{\text{siw}} + \beta_m L_m \tag{6}$$

Based on the above principle, a substrate integrated waveguide (SIW) unequal power divider with an axisymmetric structure was constructed, with the output current ratio set as $I_2 : I_3 : I_4 : I_5 = 0.58 : 0.66 : 0.88 : 1$. Fig. 6 presents the simulated S-parameters of the eight-way unequal divider applied to the array feeding network. Within the frequency range of 77–81 GHz, S_{11} remains below -10 dB, reaching -26.55 dB at 79 GHz, which satisfies the requirements of a Chebyshev power divider.

Following the power divider, phase shifters are connected, consisting of a section of SIW transmission line and a microstrip line matched to $50\,\Omega$, enabling precise phase control for output ports 2–9. As shown in Fig. 7, this design achieves phase synchronization at the operating frequency of 79 GHz.

3. RESULTS AND DISCUSSION

As shown in Figs. 8(a) and (b), a prototype of the proposed 8×28 planar array antenna was fabricated and measured in a compact anechoic chamber. The radiation patterns and S_{11} were characterized using a 79 GHz excitation source, a standard horn antenna as the transmitter, and a WR-10 waveguide transition connected to an Agilent N5244 Vector Network Analyzer (VNA). The received signals were down-converted to an intermediate frequency for data acquisition and processing.

The simulated and measured reflection coefficients (S_{11}) of the 8×28 array around 79 GHz are presented in Fig. 9. Within the 77–81 GHz band, the measured return loss remains below -10 dB, with a minor frequency shift attributed to fabrication tolerances and waveguide-to-microstrip transition. The measured impedance bandwidth is 8.86% (75.2–82.2 GHz). The phase characteristics at the ports meet the design specifications, ensuring low-sidelobe performance.

Figures 10 and 11 present broadband radiation patterns of the 8×28 planar array at 79 GHz. In the E-plane, the sidelobe level (SLL) remains below -18 dB with a flattened plateau at -11 dB and a half-power beamwidth (HPBW) of 9°. In the H-plane, SLL is below -20 dB with an HPBW of 12°, indicating effective sidelobe suppression. A slight elevation of the sidelobe in the E-plane and a beam deviation of $+1.6°$ at 79 GHz are observed, which are attributed to phase variations from amplitude fluctuations and minor feed structure imperfections. Overall, the measured radiation patterns closely match the design specifications, confirming the expected performance of the planar array antenna.

Figure 12 presents the simulated and measured gains of the 8×28 planar array. Within the operating frequency range of 77–

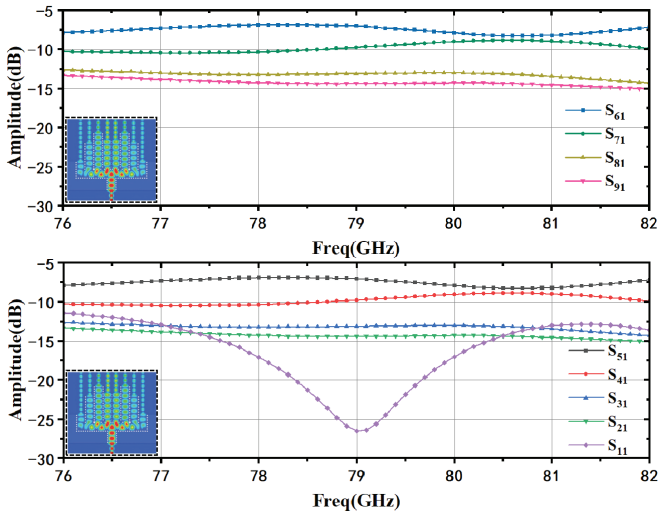

FIGURE 6. SIW feeding network S-parameter and electric field distribution diagram.

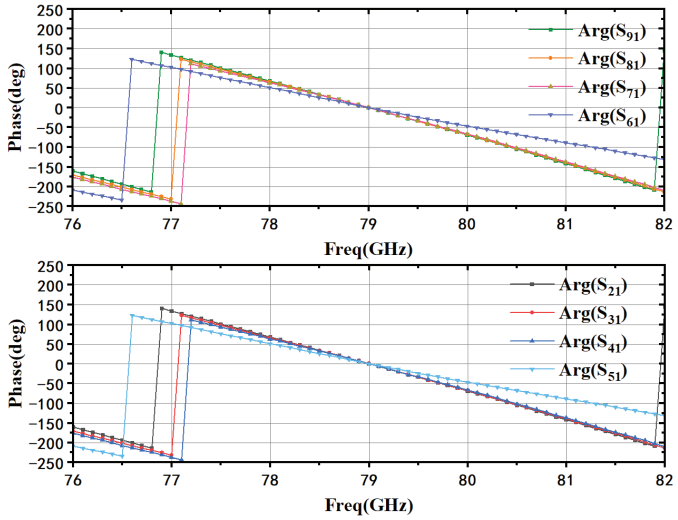

FIGURE 7. SIW feeding network S-parameter phase distribution diagram.

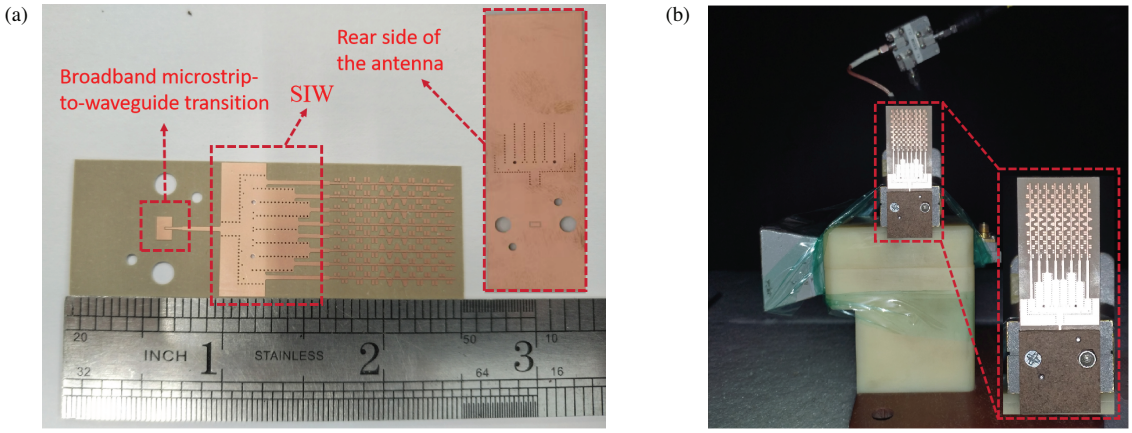

FIGURE 8. Photographs:(a) 8×28 planar array, (b) measurement setup in anechoic chamber.

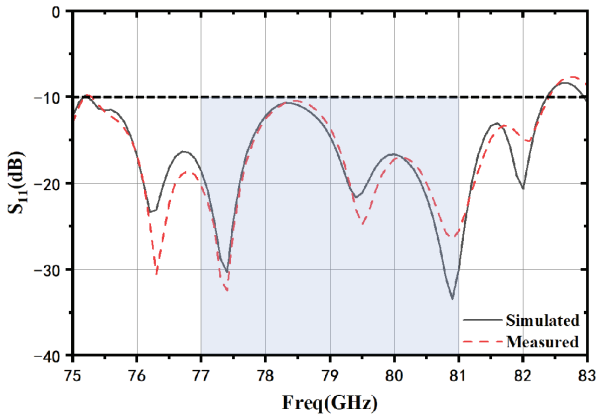

FIGURE 9. Simulation and measurement of S_{11} for 8×28 planar array antenna.

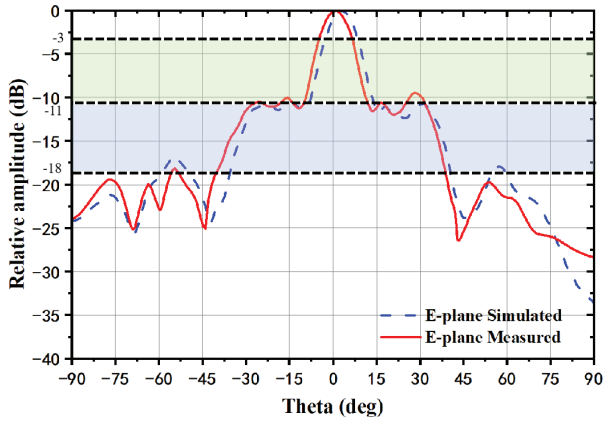

FIGURE 10. E-plane radiation pattern of the fabricated 8×28 array.

81 GHz, the measured gain of the array remains above 19.8 dBi, reaching a peak of 20 dBi with variations within 1 dB. The difference between simulation and measurement is within 1–2 dB, primarily due to fabrication tolerances. The gain stability is attributed to the closely coupled radiating elements and SIW feeding network.

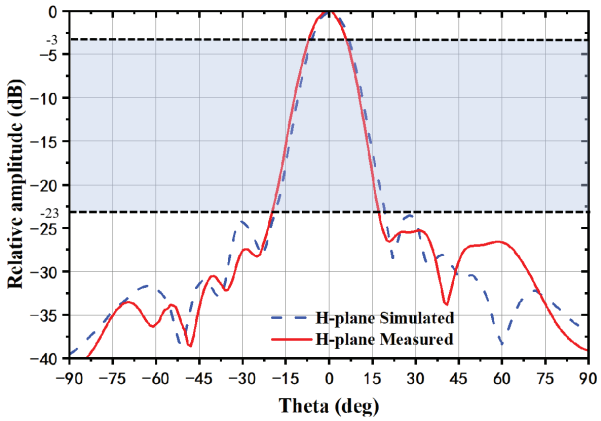

FIGURE 11. H-plane radiation pattern of the fabricated 8×28 array.

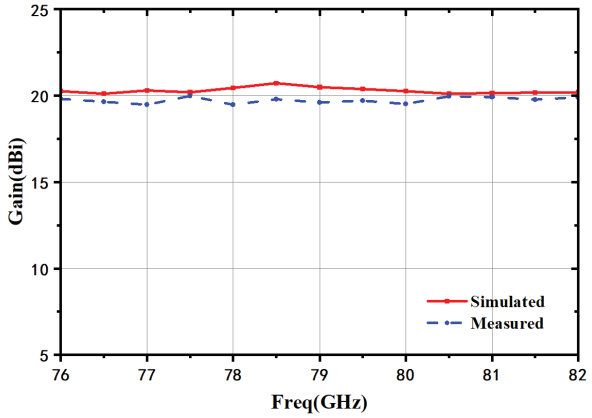

FIGURE 12. Comparison between simulated and measured gains of the 8×28 planar antenna.

TABLE 1. Performance comparison of antenna arrays.

Reference	Array Type	Frequency (GHz)	Impedance BW (%)	Peak Gain (dBi)	Layers	Detection Range
2019/[3]	6×10	77.00	6.31	14.10	1	Medium-Long
2017/[12]	6×7	28.00	6.31	12.21	2	Medium
2018/[17]	8×8	35.00	2.00	14.70	1	Long
2018/[23]	6×16	77.00	3.70	13.96	1	Medium-Long
2024/[24]	12×8	77.00	1.7	13	1	Medium
2025/[25]	16×16	21.00	3.55	17	1	Long
2020/[26]	32×32	77.00	1.3	24.4	1	Long
This Work	8×28	79.00	8.86	20.00	1	Medium-Long

Table 1 compares the proposed 8×28 planar array with existing designs. The proposed array achieves a wide impedance bandwidth of 8.86% and a high peak gain of 20 dBi using a single-layer substrate, outperforming single-layer arrays in [3, 17, 23, 24] and avoiding the complexity of multilayer designs in [12] and [25]. Compared with large-element arrays with limited bandwidth, such as [26], it provides a balanced trade-off among bandwidth, gain, and integration. By employing an SIW feeding network, the design expands the bandwidth while maintaining stable radiation, offering a compact, high-performance solution suitable for millimeter-wave vehicle-mounted radar systems requiring medium-to-long detection ranges and high integration.

4. CONCLUSION

A broadband millimeter-wave antenna array employing SIW feeding and proximity-coupled radiating elements has been presented for integrated mid- and long-range automotive radar in the 77–81 GHz band. The design leverages hybrid patch geometry, standing-wave excitation, and reflective slots to achieve broadband impedance matching, stable radiation, and suppressed sidelobes. Experimental measurements show close agreement with simulations, confirming the effectiveness of the proposed array architecture. These results demonstrate its potential for high-resolution radar applications requiring compact, integrated, and broadband antenna solutions.

REFERENCES

[1] Zang, Z., Q. Ren, A. U. Zaman, and J. Yang, "77 GHz fully polarimetric antenna system with compact circularly polarized slots in gap waveguide for automotive radar," *IEEE Transactions on Antennas and Propagation*, Vol. 72, No. 7, 5578–5588, 2024.

[2] Kung, M.-L., J.-Y. Yu, K.-H. Lin, C.-H. Chen, H.-H. Cheng, C.-Y. Wu, Y.-H. Tien, and Y.-C. Ding, "Antenna in package with tapered radiation patches and parasitic strips for automotive radar," *IEEE Antennas and Wireless Propagation Letters*, Vol. 23, No. 10, 2845–2849, 2024.

[3] Dokhanchi, S. H., M. R. B. Shankar, K. V. Mishra, T. Stifter, and B. Ottersten, "Performance analysis of mmWave bi-static PMCW-based automotive joint radar-communications system," in *2019 IEEE Radar Conference (RadarConf)*, 1–6, Boston, MA, USA, 2019.

[4] Hasch, J., E. Topak, R. Schnabel, T. Zwick, R. Weigel, and C. Waldschmidt, "Millimeter-wave technology for automotive radar sensors in the 77 GHz frequency band," *IEEE Transactions on Microwave Theory and Techniques*, Vol. 60, No. 3, 845–860, 2012.

[5] Shin, D.-H., K.-B. Kim, J.-G. Kim, and S.-O. Park, "Design of null-filling antenna for automotive radar using the genetic algorithm," *IEEE Antennas and Wireless Propagation Letters*, Vol. 13, 738–741, 2014.

[6] Sun, J., "A novel design of 45 linearly polarized array antenna with taylor distribution," *Progress In Electromagnetics Research Letters*, Vol. 106, 151–155, 2022.

[7] Yang, T., Z. Zhao, D. Yang, and Z. Nie, "Low cross-polarization SIW slots array antenna with a compact feeding network," *IEEE Antennas and Wireless Propagation Letters*, Vol. 20, No. 2, 189–193, 2021.

[8] Ku, B.-H., P. Schmalenberg, O. Inac, O. D. Gurbuz, J. S. Lee, K. Shiozaki, and G. M. Rebeiz, "A 77-81-GHz 16-element phased-array receiver with ±50° beam scanning for advanced automotive radars," *IEEE Transactions on Microwave Theory and Techniques*, Vol. 62, No. 11, 2823–2832, 2014.

[9] Karimipour, M. and A. Pirhadi, "A novel approach to synthesis of non-uniform conformal reflectarray antennas," *Applied Computational Electromagnetics Society Journal (ACES)*, Vol. 28, No. 11, 1040–1049, 2013.

[10] Qian, J., H. Zhu, M. Tang, and J. Mao, "A 24 GHz microstrip comb array antenna with high sidelobe suppression for radar sensor," *IEEE Antennas and Wireless Propagation Letters*, Vol. 20, No. 7, 1220–1224, 2021.

[11] Wei, W. and X. Wang, "A 77 GHz series fed weighted antenna arrays with suppressed sidelobes in E-and H-plane," *Progress In Electromagnetics Research Letters*, Vol. 72, 23–28, 2018.

[12] Xu, J., W. Hong, H. Zhang, G. Wang, Y. Yu, and Z. H. Jiang, "An array antenna for both long-and medium-range 77 GHz automotive radar applications]," *IEEE Transactions on Antennas and Propagation*, Vol. 65, No. 12, 7207–7216, 2017.

[13] Li, Y., S. Xie, and S. Xiao, "A modular wideband dual CP tightly coupled phased array antenna with 70° scanning," *IEEE Transactions on Antennas and Propagation*, 2025.

[14] Jabbar, A., J. U.-R. Kazim, Z. Pang, M. A. B. Abbasi, Q. H. Abbasi, M. A. Imran, and M. Ur-Rehman, "A wideband frequency beam-scanning antenna array for millimeter-wave industrial wireless sensing applications," *IEEE Sensors Journal*, Vol. 24, No. 8, 13 315–13 325, 2024.

[15] Diawuo, H. A. and Y.-B. Jung, "Broadband proximity-coupled microstrip planar antenna array for 5G cellular applications," *IEEE Antennas and Wireless Propagation Letters*, Vol. 17, No. 7, 1286–1290, 2018.

[16] Saeed, M. A. and A. O. Nwajana, "Design of a rectangular linear microstrip patch antenna array for 5G communication," in *2024 IEEE International Symposium on Phased Array Systems and Technology (ARRAY)*, 1–4, Boston, MA, USA, 2024.

[17] Dzagbletey, P. A. and Y.-B. Jung, "Stacked microstrip linear array for millimeter-wave 5G baseband communication," *IEEE Antennas and Wireless Propagation Letters*, Vol. 17, No. 5, 780–783, 2018.

[18] Lee, J.-H., J. M. Lee, K. C. Hwang, D.-W. Seo, D. Shin, and C. Lee, "Capacitively coupled microstrip comb-line array antennas for millimeter-wave applications," *IEEE Antennas and Wireless Propagation Letters*, Vol. 19, No. 8, 1336–1339, 2020.

[19] Xu, F. and K. Wu, "Guided-wave and leakage characteristics of substrate integrated waveguide," *IEEE Transactions on Microwave Theory and Techniques*, Vol. 53, No. 1, 66–73, 2005.

[20] Zhang, W., Z. Shen, K. Xu, and J. Shi, "A compact wideband phase shifter using slotted substrate integrated waveguide," *IEEE Microwave and Wireless Components Letters*, Vol. 29, No. 12, 767–770, 2019.

[21] Ji, Y., L. Ge, J. Wang, Q. Chen, W. Wu, and Y. Li, "Reconfigurable phased-array antenna using continuously tunable substrate integrated waveguide phase shifter," *IEEE Transactions on Antennas and Propagation*, Vol. 67, No. 11, 6894–6908, 2019.

[22] Cheng, Y. J., H. Xu, D. Ma, J. Wu, L. Wang, and Y. Fan, "Millimeter-wave shaped-beam substrate integrated conformal array antenna," *IEEE Transactions on Antennas and Propagation*, Vol. 61, No. 9, 4558–4566, 2013.

[23] Yu, Y., W. Hong, H. Zhang, J. Xu, and Z. H. Jiang, "Optimization and implementation of SIW slot array for both medium-and long-range 77 GHz automotive radar application," *IEEE Transactions on Antennas and Propagation*, Vol. 66, No. 7, 3769–3774, 2018.

[24] Nabi, R., L. Wei-Jun, and M. R. Majeed, "Design of microstrip array antenna for vehicle millimeter wave radar," *European Journal of Electrical Engineering and Computer Science*, Vol. 8, No. 2, 77–90, Apr. 2024.

[25] Sun, D.-M., W.-Y. Liu, Z.-C. Hao, and S. Gao, "A 6-21 GHz dual-polarized planar wide-scanning phased array antenna for upper mid-band 6G applications," *IEEE Transactions on Antennas and Propagation*, 2025.

[26] Yasini, S., K. Mohammadpour-Aghdam, and M. Mohammad-Taheri, "Low-cost comb-line-fed microstrip antenna arrays with low sidelobe level for 77 GHz automotive radar applications," *Progress In Electromagnetics Research M*, Vol. 94, 179–187, 2020.